NUMERICAL INVESTIGATION OF THE SEPARATED FLOW OVER A SMOOTHLY CONTOURED RAMP

Bono Wasistho*
Mechanical and Aerospace Engineering Department
Arizona State University
Tempe, Arizona 85287-6106, USA
wasistho@galileo.cse.uiuc.edu

Kyle D. Squires
Mechanical and Aerospace Engineering Department
Arizona State University
Tempe, Arizona 85287-6106, USA
squires@asu.edu

ABSTRACT

Large Eddy Simulation (LES) and Reynolds-averaged Navier-Stokes (RANS) calculations have been used to predict the development, separation, reattachment and downstream recovery of the flow over a smoothly contoured ramp. The statistically two-dimensional upstream flow separates along the ramp surface and then reattaches downstream on a flat section. A canonical flat-plate turbulent boundary layer at a momentum thickness Reynolds number 1100, and having a boundary layer thickness $0.13L_r$, is introduced four ramp lengths upstream of the onset of curvature. Subgrid-scale (SGS) stresses in the LES are closed using the dynamic eddy viscosity model of Germano *et al.* (1991). RANS calculations of the steady-state solution are performed using two leading models: Spalart-Allmaras (Spalart-Allmaras 1994) and v^2-f (Durbin 1991). Mean flow predictions obtained using all the models agree well with the experimental measurements of Song *et al.* (2000). Boundary layer detachment occurs along the curved section ($x/L_r \approx 0.4$) with reattachment at roughly $x/L_r \approx 1.4$. The primary turbulent shear stress sharply increases in the separated region and LES predictions of the shear stress development are accurate. RANS estimations of the shear stress are below the data in the separated region, though reasonable further downstream.

INTRODUCTION AND OBJECTIVES

Separated boundary layers are a challenging subset of flows that may be generally classified as 'non-equilibrium'. Non-equilibrium boundary layers are the norm, rather than the exception, in engineering applications. The importance of additional length scales to describing the flow and/or a significant imbalance between production and dissipation are two features which characterize these flows. An adverse pressure gradient boundary layer approaching separation develops an inflection point, the height of which is an additional important length scale. Turbulent stresses, for example, develop large peaks around the inflection point and boundary layer recovery following reattachment should be expected to be sensitive to this length scale.

These and other features of separated flows substantially challenge predictive methods. The vast majority of engineering predictions are obtained from solutions of the Reynolds-averaged Navier-Stokes (RANS) equations. In flows not far from equilibrium, the boundary conditions that define large scale structures remain nearly unchanged and the leading RANS models are typically adequate.

In separated flows, however, RANS models often yield mixed results (e.g., see Apsley and Leschziner 1999), providing one rationale for use of techniques such as Large Eddy Simulation (LES). In LES, the large, energy-containing scales of motion are resolved on the mesh and only the small, subgrid scales are modeled. LES predictions are less sensitive to modeling errors than their RANS counterparts. This feature should be an advantage in prediction of flows far from the calibration range of RANS models and in regimes with multiple perturbations (e.g., in pressure gradient, streamline curvature, roughness, etc.).

Assessment of simulation techniques for predicting separated boundary layers is complicated

*current address: Center for Simulation of Advanced Rockets, University of Illinois, Urbana, Illinois 61801, USA

by the fact that there is relatively strong coupling between the freestream and boundary layer. This in turn increases the sensitivity of the flow to parameters not directly connected to the turbulence model and may not allow one to easily isolate the cause of discrepancies between numerical simulation and experiment. Therefore, it is useful in any study directed towards refined evaluation of techniques and models that careful evaluation of a baseline case be established.

One of the overall aims in this work is prediction of the effect of Reynolds number on separated boundary layers (see also Song and Eaton 2001 in this volume). In the present contribution the flow at moderate Reynolds number is predicted using LES and RANS in order to assess the accuracy of each technique as well as to investigate some of the underlying characteristics of the flow. The particular flow under consideration is the statistically two-dimensional boundary layer which separates over a smoothly contoured ramp (Figure 1). The location of boundary layer detachment is not fixed by the geometry and the flow provides a reasonably well-defined platform for investigating the processes of reattachment and downstream recovery. Experimental measurements from Song *et al.* (2000) are used to evaluate the predictions.

SIMULATION OVERVIEW

The ramp geometry is shown in Figure 1. As shown in the figure, the origin of the coordinate system is fixed to the onset of the contoured section. The ramp is a portion of a circular arc in which the vertical extent is roughly one-third of the streamwise length, L_r. The reference boundary layer thickness measured upstream of the onset of curvature was about 13% of the ramp length. For other details of the experimental setup the reader is referred to Song *et al.* (2000).

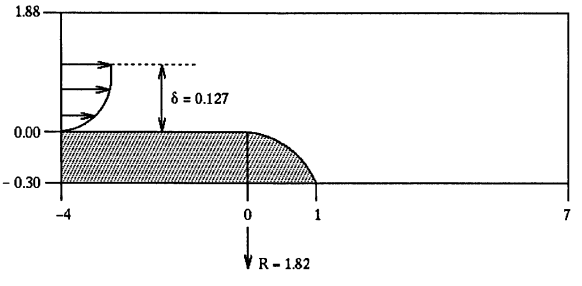

Figure 1: Ramp schematic. Curved section formed by a portion of a circular arc (note the enlarged vertical scale). Lengths in the figure and throughout have been non-dimensionalized by the ramp length L_r.

Experimental measurements are available at several streamwise locations, beginning at $x/L_r = -2$. As discussed in the next section (c.f., Figure 2), the downstream effects (pressure gradient and curvature) are already significant enough that prescribing an inflow signal in the simulations that did not exhibit an unphysical adjustment was difficult. Consequently, the simulation domain was extended two ramp lengths further upstream ($x_{in}/L_r = -4$) which was sufficient to ensure that inflow signals did not undergo arbitrary adjustment.

Predictions presented in this manuscript are obtained using Large Eddy Simulation (LES) and from the Reynolds-averaged Navier-Stokes (RANS) equations. In both approaches, an eddy viscosity hypothesis is used to close the subgrid-scale stress in the LES and Reynolds stress in the RANS. Two of the leading linear eddy viscosity models are employed in the RANS calculations: Spalart-Allmaras (referred to as 'S-A' throughout) (Spalart & Allmaras 1994) and $\overline{v^2}$–f (Durbin 1991). The dynamic Smagorinsky model is used in the LES (Germano *et al.* 1991).

In the dynamic model an expression is derived for the model coefficient via application of a "test filter" to the resolved field (applied at a scale twice as large as the grid scale). An expression for the model coefficient can be derived and evaluated during the course of the simulation. The advantage of this approach is that the model coefficient is not specified *a priori*, but rather is sensitive to local variations in the flow. On the other hand, the expression for the model coefficient can be ill-conditioned and requires spatial averaging over the statistically homogeneous spanwise direction to maintain numerical stability. Negative values of the model coefficient imply a backscatter of energy from the subgrid to resolved scales of motion and are accounted for in the dynamic procedure, albeit in an average sense. To avoid numerical instability, negative values of the subgrid viscosity were truncated to zero.

The numerical approach is based on solution the incompressible Navier-Stokes equations using a fractional step method (e.g., see Choi *et al.* 1993, Wu and Squires 1998). The present calculations are "2.5D", i.e., a curvilinear geometry in the x-y plane but with a uniform spanwise (z) coordinate along which periodic boundary conditions are applied. The homogeneous spanwise coordinate improves statistical sample, but does introduce the spanwise period as a parameter of the calculation. In the present simulations, the spanwise domain length is $4\delta_{in}$ where δ_{in} is the boundary layer thickness at the inflow plane. Two-point correlations showed this spanwise period is adequate.

The LES calculations were performed using a grid of $484 \times 60 \times 101$ mesh points in the streamwise, wall-normal, and spanwise directions, re-

spectively. The RANS grid was 323 × 53 and refinement studies showed this is sufficient, yielding less than a 2% change in the peak skin friction compared to runs on a mesh coarser by a factor of two compared to the one used to obtain the results presented here. Partial grid refinement was also conducted in the LES, though an exhaustive study with sufficient time sampling to allow a thorough evaluation of grid-size effects was not possible.

In the calculations a statistically two-dimensional turbulent boundary layer is introduced at $x_{in}/L_r = -4$, corresponding to roughly 30 inflow boundary layer thicknesses (c.f. Figure 1). The LES inflow condition was prescribed using the technique developed by Lund *et al.* (1998). In this approach, an auxiliary simulation is performed of a canonical flat-plate boundary layer, with the results at a specified plane stored for subsequent use in the ramp calculation.

As discussed further in the next section, a shallow separation occurs in the curve with reattachment in the vicinity of $x/L_r = 1.4$. From the merger of the curved and downstream flat sections, the computational domain extends $6L_r$ downstream in the LES, slightly longer in the RANS. The vertical dimension of the computational domain was the same as that in the experiments. In the LES, a zero stress condition is applied along this boundary, while in the RANS the boundary layer was resolved along the upper wall. The LES therefore does not account for the blockage from the upper wall, which affects predictions of the pressure distribution (c.f., Figure 2).

At the exit plane of the computational domain ($x/L_r = 7$) a convective boundary condition was used, identical to that employed in related studies (e.g., see Wu and Squires 1998). The grid was generated using the direct grid distribution control technique of Thomas and Middlecoff (1980).

Calculations are performed for a momentum thickness Reynolds number, Re_θ, in the boundary layer at the inlet plane of 1100. This Reynolds number permits direct resolution of the wall layer in the LES with grid spacings fine enough to minimize modeling errors. The streamwise grid spacing in the LES is less than 80 wall units, the spanwise spacing is about 25 wall units (based on the friction velocity at the inflow boundary). These grid spacings are commensurate with related applications of LES to complex boundary layers which also resolved the wall layer (e.g., see Kaltenbach *et al.* 1999). SGS modeling errors are small (peak model stress contributions are everywhere less than 10% of the resolved stress). Because the LES is well resolved the calculation database provides a detailed description of the flow which complements the experimental measurements and also permits detailed evaluation of the RANS predictions.

RESULTS

The pressure and skin friction coefficients along the lower wall from Song *et al.* (2000), along with the simulation results are shown in Figure 2 and Figure 3, respectively. From about $x/L_r = -2$, the pressure gradient is first favorable due to streamline curvature with the minimum in C_p measured and predicted just downstream of the onset of the curved section. The minimum C_p is not as deep in the LES with the slip condition applied along the upper wall, whereas both RANS models, with no-slip upper walls, provide accurate predictions. Downstream of $x/L_r = -2$, the skin friction in Figure 3 responds to the curvature by increasing from its inlet value with the maximum attained near the onset of the ramp.

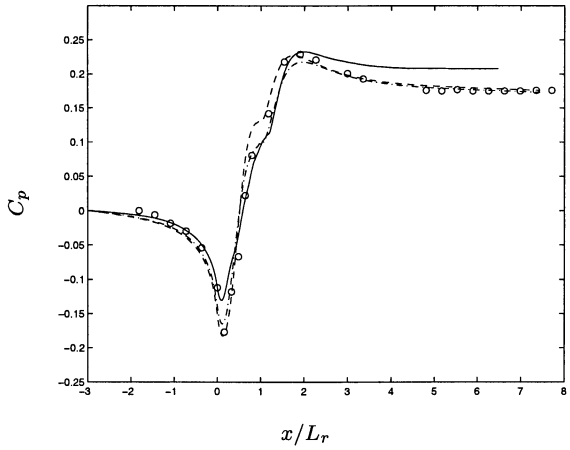

Figure 2: Pressure coefficient. ——— LES; - - - - S-A; —·— $\overline{v^2}$–f; o Song *et al.* (2000).

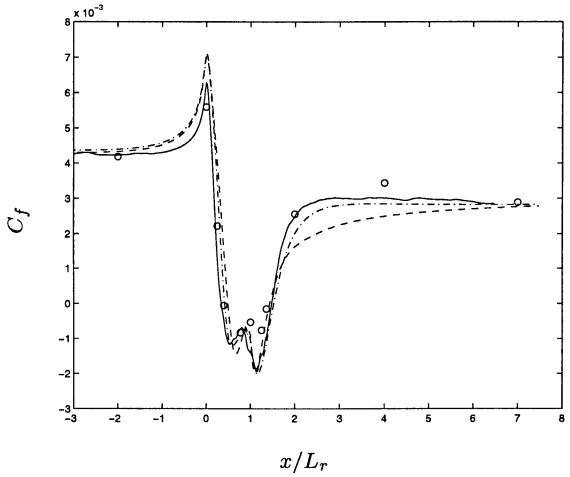

Figure 3: Skin friction coefficient. ——— LES; - - - - S-A; —·— $\overline{v^2}$–f; o Song *et al.* (2000).

The pressure gradient subsequently becomes strongly adverse and Figure 3 shows separation in

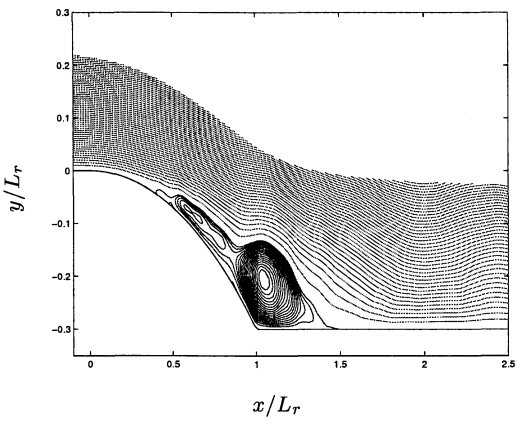

Figure 4: Streamlines in the vicinity of the recirculating region. Note the expanded vertical scale.

the mean at $x/L_r \approx 0.4$. The LES and RANS yield similar predictions of the separation location with slightly earlier detachment found in the LES. The two C_f minima in the separated region and behavior in C_p around $x/L_r = 1$ are related to the structure of the separated region. Streamlines in the vicinity of the separation zone in Figure 4 show that the reverse-flow region is comprised of two main recirculating motions: a primary recirculation at the merger of the curved and flat sections and a smaller secondary zone upstream.

Figure 3 shows that reattachment in the mean takes place around $x/L_r \approx 1.4$. In general, LES predictions of the skin friction are in the most favorable agreement with measurements in the recovery region, with the RANS predictions exhibiting a slower recovery in C_f. Note also that the downstream values of C_p are over-predicted in Figure 2, again showing the influence of the upper-wall boundary condition. Though not shown here, RANS predictions using no-stress conditions along the upper surface yield C_p distributions nearly the same as the present LES.

Figure 5 shows the time history of the separation and reattachment positions (averaged over the spanwise dimension). Fluctuations in the separation position occur at higher frequencies and exhibit smaller streamwise variations than the lower frequency observed in the reattachment location. Both the separation and reattachment trajectories in Figure 5 indicate that the separation/reattachment process is inherently unsteady and characterized by rather abrupt shedding events. Contours of the vorticity magnitude in curvilinear planes shown in Figure 6 provide another view of the flow. Close to the wall (top frame, $y/\delta_{in} = 0.018$) the vorticity field is stretched in the streamwise direction with the contours becoming more isotropic within the recirculation region and then recovering the elongated shape further downstream. This behavior is still apparent at the mid-position (middle frame, $y/\delta_{in} = 0.08$). The (curvilinear) plane at $y/\delta_{in} = 0.26$ shows significantly more activity in the vorticity field downstream of separation than in either of the planes closer to the wall. Thus, while Figure 5 provides evidence that the separation and reattachment processes are characterized by 'periodic' sheddings, Figure 6 indicates that there does not appear to be a structure of considerable spanwise coherence that dominates the separation process.

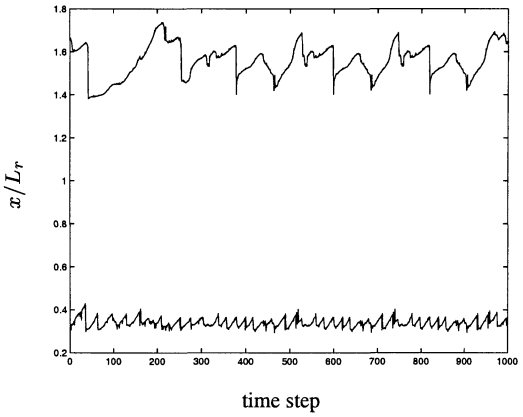

Figure 5: Temporal development of the separation and reattachment locations in the LES.

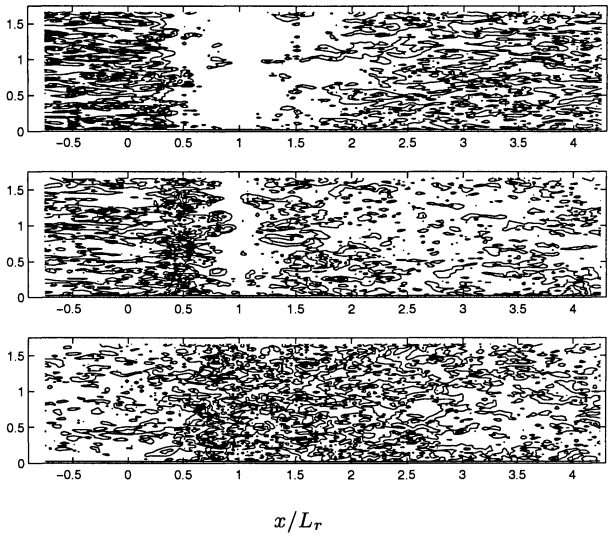

Figure 6: Contours of the vorticity magnitude in curvilinear planes $y/\delta_{in} = 0.018$ (top frame), 0.08 (middle frame), and 0.26 (bottom frame) where δ_{in} is the boundary layer thickness at the inflow plane.

Profiles of the streamwise mean velocity are shown in Figure 7. The upper frame shows profiles covering the entire streamwise extent of the calculation while the lower frame shows measurements and simulation results in the vicinity of the separation region. In general, the figure shows that both LES and RANS predictions of the mean streamwise flow are in good agreement with the measurements of Song *et al.* (2000). Boundary layer deceleration and separation are accurately predicted, as already discussed in reference to Figure 3. The

lower frame in Figure 7 provides an illustration of the relatively shallow nature of the separation. The peak backflow velocity is on the order of 10% of the freestream value and is well predicted by all the simulations. While the region of reversed flow is relatively shallow, the perturbation applied by boundary layer detachment/reattachment is relatively strong. Though not obvious from the figure, the mean profile at the furthermost streamwise position, $x/L_r = 7$ (≈ 45 inlet boundary layer thicknesses from the reattachment location), has not yet recovered the logarithmic law.

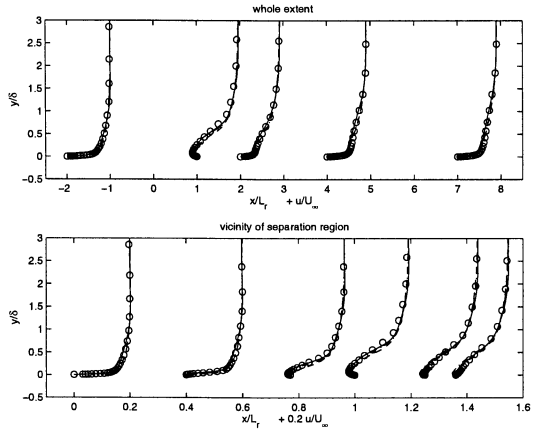

Figure 7: Mean streamwise velocity. ——— LES; - - - - S-A; —·— $\overline{v^2}$–f; ○ Song *et al.* (2000).

Shown in Figure 8 are predictions of the turbulent shear stress from the LES and RANS, compared to the experimental measurements of Song *et al.* (2000). As with the mean flow, the upper frame shows the entire streamwise extent while the lower frame focuses on the profiles in the separation region. At $x/L_r = 0.25$, the adverse pressure gradient has raised the peak shear stress compared to the inlet value with all the simulations accurately predicting the profile. In the reverse flow region the peak shear stress increases further, with its peak shifted from the wall, characteristic of adverse pressure gradient and separated boundary layers (e.g., see Simpson 1989). Note that while the shear stress levels are accurately predicted in the LES, Figure 8 shows that the RANS predictions underestimate the shear stress by about a factor of two. Though not shown here, the underestimation is linked to relatively low eddy viscosity levels in the RANS (nearly a factor of five smaller towards the downstream stations).

One view of the distortion and recovery process is shown in Figure 9. Plotted is the downstream development of the streamwise fluctuating velocity. In Figure 9a the adverse pressure gradient raises the velocity fluctuation with the peak value also further from the wall. The profiles in Figure 9b are within the reverse-flow region and then also in the

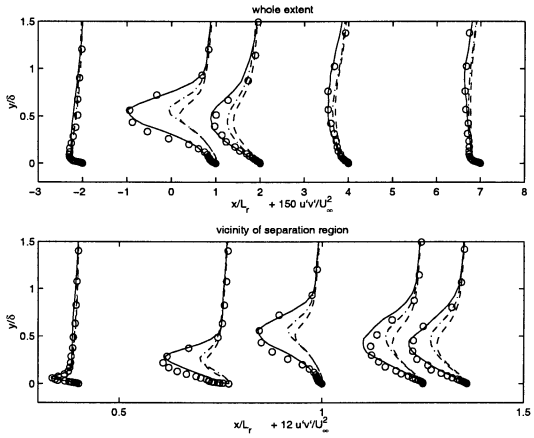

Figure 8: Primary turbulent shear stress. ——— LES; - - - - S-A; —·— $\overline{v^2}$–f; ○ Song *et al.* (2000).

recovery region following reattachment. The reattaching boundary layer recovers through growth of an inner layer (evident by $x/L_r = 2$) as well as through decay of the elevated stress levels in the outer region. As commented previously in relation to the mean flow, Figure 9 shows that by $x/L_r = 7$ the fluctuating velocity has not yet recovered to its upstream state. Thus, the recovery process is comprised of two mechanisms: development and growth of an inner layer following reattachment and decay of elevated stress levels in the outer layer.

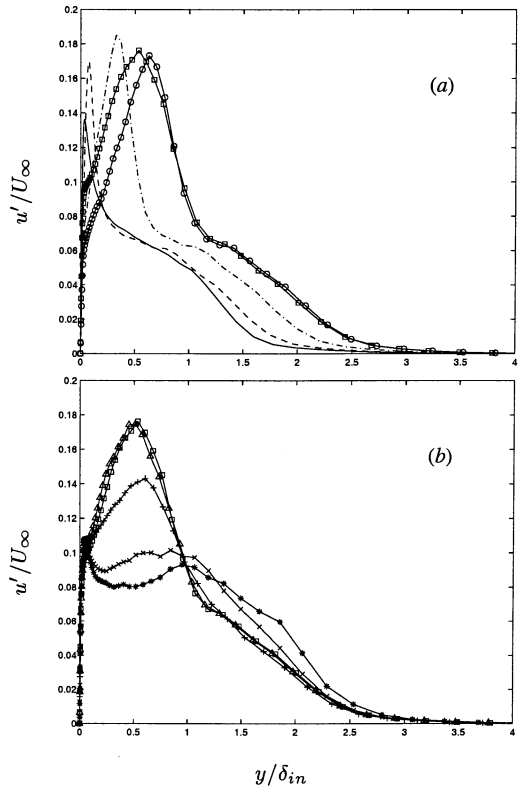

Figure 9: Development of streamwise velocity fluctuations. (*a*) x/L_r : ——— −2.00; - - - - 0.00; —·— 0.40; ○ 0.77; □ 1.00. (*b*) x/L_r : □ 1.00; △ 1.25, + 2.00; × 4.00, ∗ 7.00.

SUMMARY

Large eddy simulation and Reynolds-averaged Navier-Stokes calculations have been applied to prediction of the spatial development, separation, reattachment and downstream recovery of the boundary layer over a smoothly contoured ramp. Overall, there is fairly good agreement between LES and RANS predictions of the mean flow and the measurements of Song *et al.* (2000).

The flow exhibits a shallow separation with the region of reverse flow about one ramp length. Time series from the LES indicate that both the separation and reattachment are characterized by (time-dependent) shedding events. This inherently unsteady feature is resolved in the LES, but is difficult to parameterize within RANS closures. That difficulty is part of the explanation for the low shear stress predictions by the RANS models, especially in the reverse-flow region (c.f., Figure 8). RANS eddy viscosity levels lagged those of the LES solutions, indicative of lower mixing in the RANS calculations. Unsteady shedding of structures from the ramp into the zone of reverse flow should enhance mixing and are also an explanation for the lag in recovery of the skin friction (c.f., Figure 3). In addition, the Boussinesq approximation, applied in both the LES and RANS, becomes less reliable as separation is approached and as the boundary layer subsequently detaches with the flow departing far from equilibrium. Given the moderate Reynolds number and relatively fine mesh resolutions the modeling error in the subgrid closure has a small effect in the LES. In the RANS predictions, however, the error is substantially greater since the turbulence model dominates the solution.

The current calculation was performed at moderate Reynolds number in order to resolve the near-wall flow and avoid the empiricism that appears inevitable with wall-layer modeling for high Reynolds number LES applications. At the substantially higher Reynolds numbers representative of applications, and for which measurements are available, it appears unavoidable that LES can be applied without also introducing more empirical input (such as the law-of-the-wall in a wall-layer model, for example). The separation between the length scale characterizing the inflection of the velocity profile and near-wall structures is substantial at high Reynolds numbers and turbulence models will need to be responsive to such effects.

Acknowledgments

This work was supported by the U.S. Office of Naval Research (Grant Number N00014-98-1-0060, Program Officers: Dr. L. Patrick Purtell and Dr. Candace Wark). The authors gratefully acknowledge valuable discussions with Professor John Eaton, Dr. Philippe Spalart, and Mr. Simon Song. The simulations were performed on the Cray J90 at the U.S. Department of Defense High Performance Computing Major Shared Resource Centers (CEWES and NAVO).

REFERENCES

Apsley, D.D., and Leschziner, M.A., 1999, "Advanced turbulence modeling of separated flow in a diffuser", *Flow, Turbulence and Combustion*, **63**, pp. 81-112.

Choi, H., Moin, P., and Kim, J., 1993, "Direct numerical simulation of turbulent flow over riblets", *J. Fluid Mech.*, **255**, pp. 503-539.

Durbin, P.A., 1991, "Near-wall turbulence closure without damping functions", *Theo. and Comp. Fluid Dynamics*, **3**, pp. 1-13.

Germano, M., Piomelli, U., Moin, P. & Cabot, W.H., 1991, "A dynamic subgrid-scale eddy viscosity model", *Phys. Fluids*, **3**, p. 1760.

Kaltenbach, H.-J., Fatica, M., Mittal, R., Lund, T.S., and Moin, P., 1999, "Study of flow in a planar asymmetric diffuser using large-eddy simulation", *J. Fluid Mech.*, **390**, pp. 151-185.

Lund, T.S., Wu, X., and Squires, K.D., 1998, "Generation of turbulent inflow data for spatially-developing boundary layer simulations", *J. Comp. Physics*, **140**(2), pp. 233-258.

Simpson, R.L., 1989, "Turbulent boundary layer separation", *Ann. Review of Fluid Mechanics*, **21**, pp. 205-234.

Spalart, P.R. and Allmaras, S.R., 1994, "A one-equation turbulence model for aerodynamic flows", *La Recherche Aerospatiale*, **1**, pp. 5-21.

Song, S., DeGraaff, D., and Eaton, J.K., 2000, "Experimental study of a separating, reattaching and redeveloping flow over a smoothly contoured ramp", *Int. J. Heat and Fluid Flow*, **21**(5), pp. 512-519.

Thomas, P.D., and Middlecoff, J.F., 1980, "Direct control of the grid point distribution in meshes generated by elliptic equations", *AIAA J.*, **18**, pp. 652-656.

Wu, X., and Squires, K.D., 1998, "Numerical investigation of the turbulent boundary layer over a bump", *J. Fluid Mech.*, **362**, pp. 229-271.